P-odd angular correlations in resonance (n,γ) reactions

V. R. Skoĭ and É. I. Sharapov
Joint Institute for Nuclear Research, Dubna

Fiz. Elem. Chastits At. Yadra **22**, 1400–1432 (November–December 1991)

The recent theoretical and experimental studies on angular and polarization correlations in the differential cross sections for radiative neutron capture with direct photon emission are reviewed. The discussion focuses on the problem of obtaining complete spectroscopic information on *p*-wave neutron resonances, including the entrance-channel mixing parameter.

INTRODUCTION

The study of the angular and polarization correlations in radiative capture reactions parallels the work on the problem of angular distributions in nuclear reactions. The involvement in a reaction of several angular momenta with the corresponding magnetic projections made the problem complex at first. However, there was an encouraging feature arising from the natural connection between the angular momentum and parity of nuclear states with their symmetry properties under spatial reflections and rotations and time reversal. In his work on the theory of atomic spectra, Wigner[1] was the first to point this out, and he used group theory to derive expressions for the angular-momentum vector-addition coefficients. In studies begun in the 1940s (Refs. 2 and 3), Racah laid the basis for the algebraic theory of the transformation functions and irreducible tensor operators introduced for describing the angular-momentum properties.

The first experimental results on the angular distributions were obtained in the late 1940s. As early as the beginning of the 1950s the fundamental studies of Fano[4] and of Coester and Jauch[5] appeared, which introduced the custom of using the density matrix of spin states and the tensor formalism. The problem of the summation over magnetic quantum numbers was solved by elegant methods which, unlike the previous ones, did not require complicated calculations. Subsequent studies by Biedenharn and Rose,[6] Simon,[7] Shirokov,[8] Huby,[9] and Goldfarb[10] completed the construction of the formalism for describing angular correlations in (n,γ) and (p,γ) reactions, and it came to be referred to as the standard theory. Without mentioning the many other studies, we note the part of the widely known book by Baldin, Gol'danskiĭ, and Rozental'[11] devoted to problems of polarization and nuclear reactions involving photons. To the reader interested in later theoretical and experimental developments we recommend the monographs of Ferguson[12] and Gill[13] on angular correlations in γ spectroscopy.

The main purpose of the experimental studies in this area was and still is to obtain spectrometric information on the nuclear levels, and also to study the mechanisms of specific nuclear reactions. The study of the angular distributions of the γ quanta of radiative capture of thermal polarized neutrons has become an independent area of research. It is in precisely this area that Abov, Krupchitsky, and Oratovsky have discovered spatial-parity nonconservation in nuclear interactions.[14] The experimental effects of these so-called *P*-odd correlations have turned out to be small, on the order of 10^{-4}, but fully measurable. The subsequent publications on this question are reviewed in Ref. 15.

In recent years there has been renewed interest in the problem of angular correlations, particularly in the spectrometry of γ quanta from *p*-wave neutron resonances. This is related to the experimental discovery in them of the enhancement of spatial-parity nonconservation effects.[16] The measured longitudinal asymmetries of the total cross sections have reached 10% (Refs. 17–20). Experiments to seek violations of the time-reversal symmetry of nuclear reactions have been proposed for these resonances.[21]

At the present time the possibilities of the theoretical interpretation of such experiments are limited by the absence of information on the spins, widths, and mixing parameters of the *p*-wave resonances in question. The angular correlations and, in particular, the *P*-even effects in them offer the possibility of obtaining such information. Below we review the latest theoretical studies devoted to *P*-even effects in the differential cross sections of resonance (n,γ) and (p,γ) reactions. The first experimental results in this area were obtained for (p,γ) reactions, and we analyze them for several examples. *P*-even angular correlations in *p*-wave neutron resonances were until recently studied only in the Laboratory of Neutron Physics at the JINR. Below we describe the technique used to make these measurements and give the few results now available for ^{117}Sn and ^{113}Cd targets. There has not yet been a consistent theoretical explanation of them within the framework of the standard resonance model. Therefore, the concluding section of this review is devoted to the discussion of additional experiments with polarized neutrons and nuclei which are needed for a "complete" experiment allowing analysis without the use of a dynamical reaction model.

1. PARAMETERS OF AN ISOLATED *p* RESONANCE. CHANNEL MIXING

A typical picture of the differential cross section of radiative neutron capture with direct γ emission is shown in Fig. 1 for a low-energy *p*-wave resonance of energy E_p. The standard parameters characterizing the resonance are its energy E_p, spin J, total width Γ, the total neutron width Γ_n, and the partial radiative width $\Gamma_{\gamma i}$ for the transition of

 0090-4759/91/060681-17$04.00

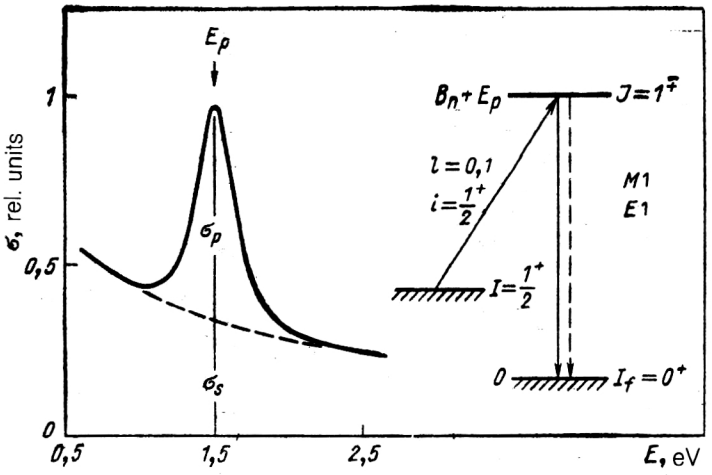

FIG. 1. Typical energy dependence of the differential cross section for radiative neutron capture near a p-wave resonance.

energy $E_{\gamma i}$. The resonance is superimposed on the smooth background of the s-wave cross section due to an adjacent s-wave resonance or direct neutron capture. The cross-section ratio $\sigma_p(\theta,E_p)/\sigma_s(\theta,E_p)$ taken at the energy $E=E_p$ is a natural experimental parameter characterizing neutron capture in states with orbital angular momenta $l=1$ and $l=0$.

Three angular momenta are involved in the entrance channel of the reaction: the particle orbital angular momentum l, the particle spin i, and the nuclear spin I. There are two commonly used angular-momentum addition schemes: the representation of the total angular momentum of the particle j and the representation of the channel spin s. However, different authors use different orders of vector addition in each of these schemes. We shall use the order shown in Fig. 1. In the j representation the wave function of angular momentum J will have the form $|(li)j,I;J\rangle$, which corresponds to the fact that the orbital angular momentum l is first in the sum $\mathbf{l}+\mathbf{i}=\mathbf{j}$, and $\mathbf{j}$ is first in the sum $\mathbf{j}+\mathbf{I}=\mathbf{J}$. In this representation the p-wave resonance is characterized by the neutron widths $\Gamma_{n1/2}$ and $\Gamma_{n3/2}$, so that the total width is $\Gamma_p=\Gamma_{n1/2}+\Gamma_{n3/2}$. This same addition scheme is also valid for the γ if we formally introduce its "orbital" angular momentum $\mathbf{l}_\gamma$ added to the photon spin $\mathbf{1}$ to form the total angular momentum usually denoted not by j, but by L: $\mathbf{l}_\gamma+\mathbf{1}=\mathbf{L}$ and $\mathbf{L}+\mathbf{I}_f=\mathbf{J}$, where L is the multipole order of the photon and I_f is the spin of the final level of the product nucleus.

In the s representation we shall write the wave function of angular momentum J as $|l,(iI)s;J\rangle$, which corresponds to addition of the orbital angular momentum l to the channel spin $\mathbf{s}$, which, in turn, is the sum $\mathbf{i}+\mathbf{I}=\mathbf{s}$. Accordingly, the two neutron widths Γ_{ns1} and Γ_{ns2} appear. For example, in the case of a target nucleus with $I=1/2$ these will be the widths Γ_{n0} and Γ_{n1}. The equation for transforming from one representation to the other in our case will have the form

$$|l,(iI)s;J\rangle=\sum_j \hat{js}W(liJI;js)\,|(li)j,I;J\rangle. \qquad (1)$$

This transformation formula was obtained by Racah in Ref. 3. The Racah coefficients $W(liJI;js)$ entering into it are tabulated in many studies, but they can also be represented analytically.[11] When the order of summation of the angular-momentum vectors is changed for a given coupling scheme, the expression (1) changes, acquiring an additional phase and a different ordering of the vectors in the argument of the Racah function. For example, the j representation of the angular momenta coupled in the form $|I,(li)j;J\rangle$ is transformed into the s representation $|(Ii)s,l;J\rangle$ according to the formula

$$|(Ii)s,l;J\rangle=\sum_j (-1)^{l+i-J}\hat{js}W(IiJl;sj)\,|I,(li)j;J\rangle, \qquad (2)$$

which is quoted in Ref. 10 with a reference to work by Satchler.

The physical quantities which can be subjected to transformations in theoretical expressions are usually the amplitudes of the neutron widths, i.e., the square roots of the corresponding widths: $\Gamma_{nj}^{1/2}$ and $\Gamma_{ns}^{1/2}$. These have recently excited particular interest because of the above-mentioned discovery of spatial-parity nonconservation in the p-wave resonances of several nuclei. In experiments with longitudinally polarized neutrons it was discovered that the total cross section contains a pseudoscalar term:

$$\sigma^{\pm}=\sigma_0(1\pm P\mathbf{s}_n\mathbf{k}_n), \qquad (3)$$

where $\sigma_0(E,E_p)$ is the p-resonance cross section for an unpolarized beam and the signs $\pm$ correspond to the two opposite projections of the neutron spin $\mathbf{s}$ on the direction of the momentum $\mathbf{k}_n$. The helical asymmetry P is defined in terms of the resonance parameters as (see, for example, Ref. 17)

$$P(E)=\frac{2H_{ps}x_{1/2}}{E-E_s}\left(\frac{\Gamma_n^s}{\Gamma_n^p}\right)^{1/2},$$
$$x_{1/2}=\frac{(\Gamma_{n1/2})^{1/2}}{(\Gamma_{n1/2}+\Gamma_{n3/2})^{1/2}}, \qquad (4)$$

where H_{ps} is the matrix element of the weak interaction between the given p- and s-wave resonances, $x\equiv x_{1/2}$ is the channel mixing parameter (henceforth we shall also use the parameter $x_{3/2}\equiv y$), and E_s and Γ_n^s are the energy and

neutron width of the s resonance. It is therefore insufficient to measure only the quantity P; it is necessary to know all the parameters of Eq. (4), including the amplitude of the neutron width $(\Gamma_{n1/2})^{1/2}$ or the mixing parameter $x_{1/2}$. Resonances with a small value of this parameter obviously do not induce a noticeable parity-violation effect even for a large value of the matrix element H_{ps}.

The effect, mentioned in the Introduction, of the P-odd asymmetry of γ emission in the direction of the neutron spin and opposite it also requires additional spectrometric information. It is described by an expression analogous to Eq. (2) with P and $\mathbf{k}_n$ replaced by P_γ and $\mathbf{k}_\gamma$. In this case the value of the P-odd asymmetry P_γ has the form (see, for example, Ref. 15):

$$P_\gamma(E)=\frac{2H_{ps}}{E_p}\left(\frac{\Gamma^p_{\gamma i}}{\Gamma^s_{\gamma i}}\right)^{1/2}A(I,J,I_f), \tag{5}$$

where $A(I,J,I_f)$ is the known spin coefficient and the amplitudes of the partial γ widths $(\Gamma^p_{\gamma i})^{1/2}$ and $(\Gamma^s_{\gamma i})^{1/2}$ and the level spin J require additional experimental determination.

These examples, which do not exhaust all the requirements on the spectroscopic information on resonances, demonstrate the need to develop real areas of fundamental research to obtain this information.

At the present time this information is clearly insufficient, which negatively affects both the interpretation of the P-odd effects and the planning of experiments. The very limited data available on the amplitudes of the widths and the channel mixing of a reaction have been obtained from the angular distributions of elastically scattered protons,[22,23] neutrons,[24] and, very rarely, γ quanta.[25] There is no such information for very weak low-energy neutron p resonances of nuclei with $A>100$. It seems to us that the only real, but very difficult, method of obtaining such information is by study of the P-even asymmetries in (n,γ) reactions near the p resonance.

2. THE THEORY OF P-EVEN ANGULAR CORRELATIONS

Using the representation of the neutron total angular momentum (see Sec. 1) and following Ref. 26, we write the differential cross section for radiative neutron or proton capture $\sigma(\theta,\varphi)$ in the form of a traditional expansion in Legendre polynomials:

$$\sigma(\theta,\varphi)=\frac{\lambda^2}{4}\left[a_0+\sum_{k\neq 0}\left(a_kP_k(\cos\theta)+b_kP_yP^1_k(\theta,\varphi)\right)\right]. \tag{6}$$

Here the z axis lies in the reaction plane and points along the beam, θ is the angle between the directions of the particle momentum $\mathbf{k}_n$ and the γ momentum $\mathbf{k}_\gamma$, φ is the azimuthal angle measured from the x axis lying in the reaction plane, P_y is the projection of the incident-particle polarization vector on the y axis, which is perpendicular to the reaction plane, and $P_k(\cos\theta)$ is a Legendre polynomial, for example,

$$P_1(\cos\theta)=\cos\theta;\quad P_2(\cos\theta)=(\tfrac{1}{2})(3\cos^2\theta-1).$$

Finally, $P^1_k(\theta,\varphi)$ is an associated Legendre polynomial, in particular,

$$P^1_1(\theta,\varphi)=\cos\theta\sin\varphi.$$

The expansion coefficients a_k and b_k are functions of the reduced matrix elements (amplitudes) of the reaction, and in our representation they have the form

$$R\equiv\langle pLI^\pi_fJ^\pi||R||lijI^\pi J^\pi\rangle. \tag{7}$$

Through these amplitudes the coefficients a_k and b_k depend on the neutron energy, the resonance parameters, and the channel mixing.

To simplify the notation in the case of capture from s and p waves with emission of γ quanta of multipole order $M1$ and $E1$ we shall use a simpler notation for the amplitudes, for example,

$$S=\langle M1\,0^+\,1^+||R||0\,\tfrac{1}{2}\,\tfrac{1}{2}\,\tfrac{1^+}{2}\,1^+\rangle;$$

$$P_{1/2}=\langle E1\,0^+\,1^-||R||1\,\tfrac{1}{2}\,\tfrac{1}{2}\,\tfrac{1^+}{2}\,1^-\rangle;$$

$$P_{3/2}=\langle E1\,0^+\,1^-||R||1\,\tfrac{1}{2}\,\tfrac{3}{2}\,\tfrac{1^+}{2}\,1^-\rangle;$$

$$|P|^2=|P_{1/2}|^2+|P_{3/2}|^2.$$

Analytic expressions for the coefficients a_k and b_k have been obtained in the form[26]

$$a_k=\sum_{tt'}(-1)^{I-I_f+1-1/2+k+j-j'}\hat{I}^{-1}\hat{i}^{-1}\hat{j}\hat{j}'\hat{l}\hat{l}'\hat{L}\hat{L}'\hat{J}^2\hat{J}^{2'}(l0,l'0|k0)\,[\tfrac{1}{2}+\tfrac{1}{2}(-1)^{k+L+p+L'+p'}]\,W(ljl'j';\tfrac{1}{2}k)$$

$$\times(L1,L'-1|k0)\,W(jJj';Ik)\,W(LJL'J';I_fk)\,\mathrm{Re}(RR'^*); \tag{8}$$

$$b_k=\frac{\sqrt{6}\hat{k}}{\sqrt{k(k+1)}}=\sum_{tt'}(-1)^{I-I_f+l'-j'}\hat{I}^{-1}\hat{l}^{-1}\hat{j}\hat{j}'\hat{l}\hat{l}'\hat{L}\hat{L}'\hat{J}^2\hat{J}^{2'}(l0,l'0|k0)\,[\tfrac{1}{2}+\tfrac{1}{2}(-1)^{k+L+p+L'+p'}]$$

$$\times(L1,L'-1|k0)\,W(jJj'J';Ik)\,W(LJL'J';I_fk)\,X(l\tfrac{1}{2}j;l'\tfrac{1}{2}j';k1k)\,\mathrm{Im}(RR'^*), \tag{9}$$

where tt' denotes summation over all symbols occurring twice, with and without the prime. In these equations we have used the standard notation for the Clebsch–Gordan coefficients in the form of parentheses $(L1, L'-1|k0)$, the $9j$ symbols are written as $X(...)$, and for $(2k+1)^{1/2}$ we write $\hat{k}$. In the numerical calculations we use the tabulated values of the $9j$ symbols and the Racah coefficients, given, for example, in Ref. 11.

As an example, let us consider neutron capture by a nucleus with spin $1/2^+$ in the state with $J=1$, which leads to the product-nucleus ground state with $I_f^\pi = 0^+$ (see Fig. 1). Only the coefficients a_0, a_1, a_2, and b_1 remain in Eq. (6). All the expressions become simpler:

$$\sigma(\theta,\varphi)=\frac{\lambda\!\!\!^{-2}}{4}\,[a_0+a_1\cos\theta+Pb_1\sin\theta\cos\varphi + a_2P_2(\cos\theta)]; \tag{10}$$

$$a_0=\frac{3}{4}\,(|S|^2+|P_{1/2}|^2+|P_{3/2}|^2); \tag{10a}$$

$$a_1=\frac{3}{4}\,\mathrm{Re}(-2SP_{1/2}^*-\sqrt{2}SP_{3/2}^*); \tag{10b}$$

$$b_1=\frac{3}{4}\,\mathrm{Im}\left(2SP_{1/2}^*-\frac{1}{\sqrt{2}}SP_{3/2}^*\right); \tag{10c}$$

$$a_2=\frac{3}{4}\left[\frac{1}{\sqrt{2}}\,(P_{1/2}P_{3/2}^*+P_{1/2}^*P_{3/2})-\frac{1}{2}\,|P_{3/2}|^2\right]. \tag{10d}$$

The overall factor of $\frac{3}{4}$ is the value of the statistical factor $g=(2J+1)/(2i+1)(2I+1)$. Although the notation for the reaction amplitude in the form (7) implies a certain parametrization, it is not related to the physical model of the process. Therefore, Eq. (10) is valid for any reaction with the values assumed in our example, namely, $l=0$ or $j=1$, $J=1$.

With these assumptions, let us now consider the case where only the p-wave amplitude of the reaction P_j has a resonance behavior, i.e., it is described by the Breit–Wigner formula

$$P_j=Bx_jP(E);\quad B=[\Gamma_n(E_0)\Gamma_{\gamma i}]^{1/2}/(\Gamma/2);$$

$$j=1/2,3/2; \tag{11a}$$

$$P(E)=\frac{(E/E_0)^{3/4}}{(E-E_0)/(\Gamma/2)+i}. \tag{11b}$$

In turn, the s-wave amplitude S has the standard energy dependence:

$$S=S(E_0)(E/E_0)^{1/4}. \tag{11c}$$

Equations (10) are easily adapted to this case. However, it is more useful to turn to the study of Ref. 27, also carried out in the j representation and devoted to polarization correlations near the p resonance. For the particular example in question the following expressions were derived in that study:

$$\sigma(\mathbf{k}_\gamma\mathbf{k}_n)=A_0+A_1(\mathbf{k}_\gamma\mathbf{k}_n)+B_1\sigma[\mathbf{k}_\gamma\mathbf{k}_n] + A_2[(\mathbf{k}_\gamma\mathbf{k}_n)^2-1/3]; \tag{12}$$

$$A_0=|u_s|^2+|u_p|^2; \tag{12a}$$

$$A_1=(-2x+\sqrt{2}y)\,\mathrm{Re}(u_su_p^*); \tag{12b}$$

$$B_1=\left(2x+\frac{1}{\sqrt{2}}y\right)\mathrm{Im}(u_su_p^*); \tag{12c}$$

$$A_2=-3\left(\frac{1}{\sqrt{2}}+\frac{1}{4}y^2\right)|u_p|^2, \tag{12d}$$

where u_s is the s-wave capture amplitude, u_p is the p-wave amplitude, given by Eq. (11b) up to a constant, and $x\equiv x_{1/2}$ and $y\equiv y_{3/2}$ are the relative amplitudes of the neutron widths for the channels $j=1/2$ and $j=3/2$ introduced in Sec. 1.

We see that Eqs. (10) and (12) differ by the sign in front of the amplitude $P_{3/2}$. This is because of the reversed order of adding the angular momenta **j** and **I**: the use of the angular function $|I,(l+i)j;J\rangle$ (Ref. 27) instead of $|(l+i)j,I;J\rangle$ for $I=1/2$, $J=1$ changes (owing to the symmetry properties of the Clebsch–Gordan coefficients) sign in states with $j=3/2$ but not in states with $j=1/2$.

Keeping for definiteness the phase conventions of Ref. 27 but using our notation for the amplitudes, we obtain expressions for P-even effects in a form convenient for comparison with experiment. The effect of the left–right asymmetry for $\theta=90°$ is described by the expression

$$\varepsilon^{\mathrm{L\text{-}R}}(90°)=\frac{\sigma(\pi/2,0)-\sigma(\pi/2,\pi)}{P_y[\sigma(\pi/2,0)+\sigma(\pi/2,\pi)]}=\frac{b_1}{a_0-a_2/2}. \tag{13}$$

The forward–backward asymmetry in the unpolarized beam is expressed as

$$\varepsilon^{\mathrm{F\text{-}B}}(\theta)=\frac{\sigma(0)-\sigma(\pi-\theta)}{\sigma(\theta)+\sigma(\pi-\theta)}=\frac{a_1\cos\theta}{a_0+a_2P_2(\cos\theta)}. \tag{14}$$

Sometimes the angular anisotropy of the p component of the cross section is also measured. It is given by

$$\varepsilon^a(\theta)=\frac{2\sigma(90°)}{\sigma(\theta)+\sigma(\pi-\theta)}=\frac{a_{0p}-a_2/2}{a_{0p}+(1/2)a_2(3\cos^2\theta-1)}. \tag{15}$$

Substituting the corresponding expressions for the expansion coefficients, we obtain, for example, the forward–backward effect

$$\varepsilon^{\mathrm{F\text{-}B}}(\theta) =\frac{(-2x+2^{1/2}y)BS_0(E/E_0)(E-E_0)}{S^2[1+\bar{\sigma}_p(\theta,E)/\sigma_s(\theta)][4(E-E_0)/\Gamma^2+1](\Gamma/2)}, \tag{16}$$

where we have introduced the notation

$$\bar{\sigma}_p(\theta,E)=P^2(E)\left[1-\left(\frac{1}{\sqrt{2}}xy+\frac{y^2}{4}\right)P_2(\cos\theta)\right]. \tag{17}$$

In experiments the cross section $\bar{\sigma}_p(\theta,E)$ is the average for the angles θ and $180°-\theta$. It does not involve the asymmetry parameter a_1. The energy dependence of the cross section is determined by the resonance denominator

$$\bar{\sigma}_p(\theta,E)=\bar{\sigma}_p(\theta,E_0)\,[4(E-E_0)^2/\Gamma^2+1]^{-1}. \qquad (18)$$

Introducing into (18) the experimental parameter corresponding to the ratio of the cross sections at the resonance maximum

$$t_\theta^2(E_0)=\sigma_p(\theta,E_0)/\sigma_s(\theta,E_0) \qquad (19)$$

and substituting (18) into (16), we obtain

$$\sigma^{\text{F-B}}=\frac{(-2x+2^{1/2}y)(B/S_0)\cos\theta(E/E_0)^{1/2}(E-E_0)/(\Gamma/2)}{4(E-E_0)^2/\Gamma^2+1+t_\theta^2E/E_0}. \qquad (20)$$

It remains only to relate the coefficient B/S_0 to the parameter t_θ^2. For this we find the theoretical expression for it using Eqs. (17) and (11) (the latter for $E=E_p$, recalling that $P_{3/2}^2+P_{1/2}^2=P^2$):

$$t^2=(B/S_0)^2[1-(xy/2^{1/2}+(y^2/4)P_2(\cos\theta)]. \qquad (21)$$

Substituting the resulting expression for B/S_0 into (20), we arrive at the final expression ($\Delta E=E-E_0$):

$$\varepsilon^{\text{F-B}}=\frac{(-x+y/2^{1/2})4t_\theta\cos\theta(E/E_0)^{1/2}(E-E_0)/\Gamma}{[1-P_2(\cos\theta)(xy/2^{1/2}+y^2/4)]^{1/2}[4\Delta E^2/\Gamma^2+1+t_\theta^2E/E_0]}. \qquad (22)$$

Proceeding in a similar manner for the left–right asymmetry, we can express it as

$$\varepsilon^{\text{L-R}}=\frac{(x+y/2^{3/2})2t_{90}(E/E_0)^{1/2}}{(1+xy/2^{1/2}+y^2/4)^{1/2}[4\Delta E^2/\Gamma^2+1+t_{90}^2E/E_0]}. \qquad (23)$$

In the subsequent equations the parameter t_θ, the square root of the quantity defined in Eq. (19), is taken with the same sign. This parameter describes the interference of the s- and p-wave amplitudes measured experimentally. However, the measurements focus on the quantities $x=(\Gamma_{n1/2}/\Gamma_n)^{1/2}$ and $y=(\Gamma_{n3/2}/\Gamma_n)^{1/2}$. For this it is useful to measure the anisotropy of the p-wave part of the cross section. It is determined by Eqs. (15), (10a), and (10d) and is related to the parameters x and y as

$$\varepsilon^a(\theta)=\frac{1+xy/2^{1/2}+y^2/4}{1-P_2(\cos\theta)(y^2+xy\cdot 2^{3/2})/2}, \qquad (24)$$

$$x^2+y^2=1. \qquad (25)$$

Up to now we have used the results of calculations carried out in the representation of the neutron total angular momentum. Sometimes it is convenient to analyze the measurements of the angular distributions in the channel-spin representation. This is particularly true of the cross sections for unpolarized neutrons, when the contributions of the spin channels are incoherent. Of course, using Eqs. (1) and (2) and their analogs, we can transform from one representation to the other. For our example the corresponding expressions have the form

$$x_1=(2/3)^{1/2}x_{1/2}+(1/3)^{1/2}x_{3/2};$$

$$x_0=-(1/3)^{1/2}x_{1/2}+(2/3)^{1/2}x_{3/2}. \qquad (26)$$

There are theoretical studies, for example, Refs. 28–30, especially devoted to this problem and carried out directly in the channel-spin representation.

For targets with spin $I=1/2$ the neutron widths of the p resonances are the sum of the widths Γ_{ns}: $\Gamma=\Sigma_s\Gamma_{ns}$, where the channel-spin index takes two values, $s=0,1$. The corresponding channel mixing parameters are defined as

$$x_1=(\Gamma_{n1}/\Gamma_n)^{1/2},\quad x_0=(\Gamma_{n0}/\Gamma_n)^{1/2}.$$

The authors of Ref. 28 derived a general analytic formula for the angular distribution of γ quanta in the polarized-neutron capture reaction. The authors worked in the channel-spin representation for the following angular-momentum coupling: $(I+i)s+l=J$. The angular distribution was obtained in the form of an expansion in spherical harmonics $Y_{kn}(\theta,\varphi)$:

$$\sigma(\theta,\varphi)=\frac{\lambda^2}{4}\sum_{tt'}(-1)^{I+I_f+l'+L'+t+k-1-s'-L-J'-i}\hat{g}\hat{t}\hat{s}\hat{s}\hat{J}^2\hat{J}'^2\hat{l}\hat{l}'\hat{L}\hat{L}'\hat{I}^{-2}\hat{k}^{-1}(t\tau g0|kn)(l0,l'0|g0)$$
$$\times(L1,L'-1|k0)W(sis'i;It)W(JLJ'L';I_fk)X(slJ;s'l'J';tgk)Y_{kn}(\theta,\varphi)\rho_{t\tau}\sqrt{4\pi}$$
$$\times[\tfrac{1}{2}+\tfrac{1}{2}(-1)^{L+p+L'+p'-k}]\langle pL||R||slJ\rangle\langle p'L'||R||s'l'J'\rangle^*. \qquad (27)$$

The new quantity here, compared with Eqs. (8) and (9), is the polarization statistical tensor $\rho_{tt'}$. For a beam polarized along the y axis there are two components, $\rho_{11} = \rho_{1-1} = i\rho_y$, and for an unpolarized beam there is one: $\rho_{00} = 1/\sqrt{2}$. In addition, the parity of an electromagnetic transition is determined differently: $p = 0$ for electric and $p = 1$ for magnetic transitions. The notation in the form (27) automatically leads to real results in a calculation. The apparent complexity of Eq. (27) is a consequence of the more general approach to the problem. The same situation occurs when the expressions from Ref. 29 are used; they were derived in the channel-spin representation for the angular distribution of γ quanta in resonance reactions for arbitrary polarization in the entrance channel.

To those who use the channel-spin representation and wish to have formulas almost ready for use, we recommend the tables of Carr and Baglin[31] for unpolarized particles and those of Laszewski and Holt[32] for polarized ones. These authors have written the expression for the differential cross section as an expansion in Legendre polynomials, for example, according to Ref. 32,

$$\sigma(\theta)=\frac{\lambda^2}{4}\hat{i}^{-2}\hat{I}^{-2}\sum_{\nu}\left[\sum_{tt'}c_{tt'}(\nu)\,\mathrm{Re}(R_t^*R_{t'})\right]P_\nu(\cos\theta), \tag{28}$$

and have tabulated the values of the coefficients $c_{tt'}(\nu)$ for many sets of particle and target quantum numbers. We shall use these tables in order to slightly complicate the example of the simplest reaction, which is analyzed in this section (see Fig. 1).

We assume that in addition to the earlier constraints of a single p resonance, a single spin $J = 1$, and only dipole γ transitions, a d-wave admixture ($l = 2$) is allowed in the s-wave "background" cross section. We denote its amplitude by D_1, noting that in our example the d wave can be only in the state with channel spin $s = 1$. The coefficients of Eq. (10) written in the s representation now have a larger number of terms:

$$a_0=\tfrac{3}{4}\left(|S_1|^2+|P_0|^2+|P_1|^2+|D_1|^2\right); \tag{28a}$$

$$a_1=\tfrac{3}{4}\,\mathrm{Re}\left(-\sqrt{6}S_1P_1^*-\sqrt{3}D_1P_1^*\right); \tag{28b}$$

$$b_1=\frac{3}{4}\sqrt{6}\,\mathrm{Im}\left[S_1\left(\frac{P_1^*}{2}-\frac{P_0^*}{\sqrt{2}}\right)-D_1\left(\frac{P_0^*}{\sqrt{2}}+\frac{P_1^*}{2}\right)\right]; \tag{28c}$$

$$a_2=\tfrac{3}{4}\left[\tfrac{1}{2}|P_1|^2-|P_0|^2-\tfrac{1}{2}|D_1|^2+\sqrt{2}\,\mathrm{Re}(S_1^*D_1)\right]. \tag{28d}$$

The interference term $S_1^*D_1$ in (28d) should be noted. It describes the anisotropy of the γ-quantum emission at neutron energies away from the p resonance. The interested reader can introduce the mixing parameter x_s ($s = 0,1$) for the p resonance into Eqs. (28), which brings them to the form (12) convenient for comparison with experiment.

3. THE (p,γ) REACTION

The forward–backward asymmetry of γ emission was first discovered and then studied for a number of nuclei by proton-spectroscopy methods. In 1949 Devons[33] gave an example of a strong effect for γ radiation of energy $E_{\gamma 0} = 17.6$ MeV in the vicinity of the resonance of energy $E_p = 440$ keV ($\Gamma = 12$ keV) in the reaction $^7\mathrm{Li}(p,\gamma)^8\mathrm{Be}$. The scheme for this reaction is almost the same as that in Fig. 1. The difference is in the values of the spin and parity of the target nucleus, namely, $I^\pi = 3/2^-$ and, accordingly, in the values of the channel spin, $s = 1$ and 2, and the γ-decay modes: an $M1$ transition at the resonance and an $E1$ transition away from it. Immediately the effect was interpreted correctly as the result of interference of the resonance p-wave and the background s-wave amplitudes for proton capture with the emission of quanta of opposite parity. The example became a part of monographs on nuclear reactions.

In recent years the measurements have been repeated many times, and in Fig. 2 we give the result of the latest study.[34] The results of the polarization experiment of Ulbricht, Arnold *et al.*[35] for this reaction (see Fig. 2) with a combined analysis of all the experimental data were published only in 1977. As can be seen from Fig. 2, the left–right asymmetry effect does not have the standard resonance form, which indicates that the background amplitude has a complicated structure. The authors of Ref. 35 gave the values of the resonance p amplitudes P_1 and

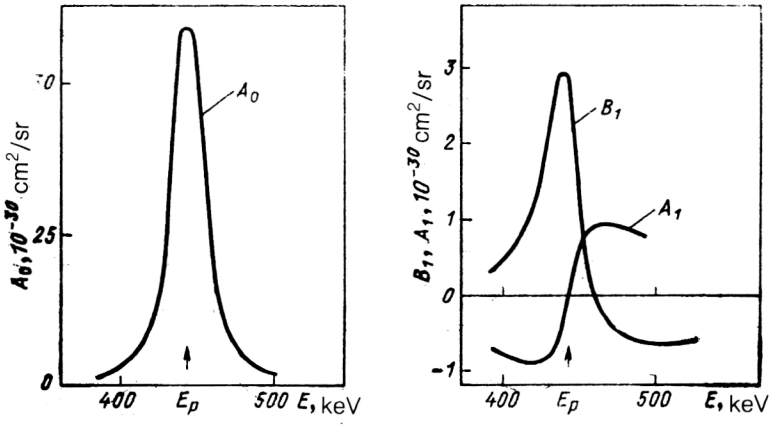

FIG. 2. Various terms [see Eq. (12)] in the differential cross section for the reaction $^7\mathrm{Li}(p,\gamma)^8\mathrm{Be}$ near the p resonance of energy $E_p = 440$ keV.

P_2 and their phase relations. In their opinion, the s-wave amplitude also has a resonance with energy greater than E_p by 60 keV. However, they did not make a direct comparison with the resonance model, and so did not notice the unphysical behavior of the phase that they obtained for the amplitude P_2 in going through the resonance. In a later analysis of these results, Barker and Ferdous[36] demonstrated the error in the signs of the polarization terms of the equations of Ref. 35. They presented arguments in favor of opposite signs of the amplitudes P_1 and P_2. The experiments and analysis have not been repeated since then.

Some years later resonance P-even effects were discovered in (p,γ) reactions on ^{12}C and ^{13}C targets. In Ref. 37 both effects were measured in the vicinity of the resonance $E_p = 14.23$ MeV. Only a single spin channel is possible for the even–even target nucleus ^{12}C. The resonance parameters $\Gamma_p = 0.8$ keV and $J^\pi = 3/2^-$ were known before, which made it possible to study the structure of the background amplitude and to show that the d wave dominates over the s wave in it, as expected theoretically for the giant-resonance region.

The results of measurements in the vicinity of another narrow resonance of the ^{12}C nucleus at energy 1.7 MeV are given by Brown *et al.* in Ref. 38. Here also large P-even effects $\varepsilon^{\text{F-B}}$ and $\varepsilon^{\text{L-R}}$ were found. After the corresponding analysis it was concluded that the experimental results can agree with the theory of angular correlations only if the amplitude of the nonresonance direct capture from the d wave in the state $D(3/2^+)$ is taken into consideration.

Interesting preliminary results for $\varepsilon^{\text{F-B}}$ and $\varepsilon^{\text{L-R}}$ in the reaction $^{13}\text{C}(p,\gamma)^{14}\text{N}$ in the vicinity of the resonance at 3.15 MeV were communicated by Weller *et al.*[39] The spin and parity of the target nucleus were $I = 1/2^-$, those of the product nucleus were $I_f = 1^+$, those of the $M1$ resonance were $J^\pi = 2^+$, and the photon energy was $E_{\gamma 0} = 10.4$ MeV. Therefore, the single spin channel $s = 0$ is involved here, but $E1$ ($M2$) and $M1$ ($E2$) multipole mixtures are possible in the exit channel. After preliminary analysis of all the experiments it was not possible to choose a unique set of amplitudes. Let us now consider the results and methods of analyzing the (p,γ) reaction amplitudes used in Ref. 40, which is devoted to study of amplitude interference effects in the giant-resonance region at higher energy.

Summarizing this section, we can state that there are still few experimental studies on P-even effects in (p,γ) spectroscopy. The only completed study specially devoted to investigation of the entrance-channel mixing in the (p,γ) reaction did not give definite results. In connection with this, the (n,γ) experiments described below become more important. So far they have been carried out by only a single group, and the publications do not contain the details of the experimental technique. Here we attempt to remedy this deficiency.

4. THE (n,γ) REACTION

Basic relations

The amplitudes of the neutron widths $\Gamma_{jn}^{1/2}$ in (n,γ) reactions can be determined from three experimental relations: the left–right asymmetry $\varepsilon^{\text{L-R}}$ in a polarized neutron beam, the forward–backward asymmetry $\varepsilon^{\text{F-B}}$ of the γ yields relative to the direction of unpolarized neutrons, and the p anisotropy of the p-wave part of the cross section ε_n^a. For measuring $\varepsilon^{\text{L-R}}$ the detector is located in the plane perpendicular to the neutron polarization vector, to the left of it and the beam direction, at an angle of 90° to the latter. At regular time intervals the polarization direction is reversed. Then $\varepsilon^{\text{L-R}}$ at the p resonance is defined as

$$\varepsilon^{\text{L-R}}(E) = [N^+(E) - N^-(E)]/[N^+(E) + N^-(E)]f_n.$$

Here $N^\pm(E)$ are the detector counts corresponding to the two directions of the beam polarization and f_n is the value of the polarization. We note that changing the sign of the polarization is equivalent to moving the detector to the right of the beam. The forward–backward asymmetry at the p resonance is measured for an unpolarized neutron beam and is defined as the difference between the numbers of γ quanta emitted from the target at angles θ and 180° $-\theta$ to the beam:

$$f(E,E') = (1/\Delta\sqrt{\pi})\exp[-(E'-E)^2/\Delta^2].$$

The anisotropy ε_p is defined as the ratio of the areas of the p resonance for the detector located at an angle of 90° to the beam and half the sum of the areas of this resonance for detectors located at the angles θ and 180° $-\theta$:

$$\varepsilon^{\text{F-B}}(\theta,E) = [N(\theta,E) - N(180^\circ - \theta,E)]/[N(\theta,E) + N(180^\circ - \theta,E)].$$

The reactors

All the experiments were carried out by the time-of-flight method in the beams of the pulsed reactors IBR-30 and IBR-2 of the Laboratory of Neutron Physics at the JINR. The IBR-30 operated in two modes: the reactor mode and the booster mode, i.e., with breeding of neutrons from the target of the linear electron accelerator LUÉ-40.

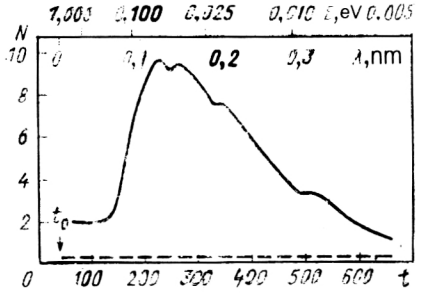

FIG. 3. Neutron spectrum of the beam filtered through a 5-cm lead filter and a 5-cm aluminum filter. On the vertical axis are counts of a detector of efficiency $\varepsilon(\lambda) = \varepsilon(\lambda_0)\lambda/\lambda_0$ in relative units; t is the number of the encoder channel of width 64 μsec.

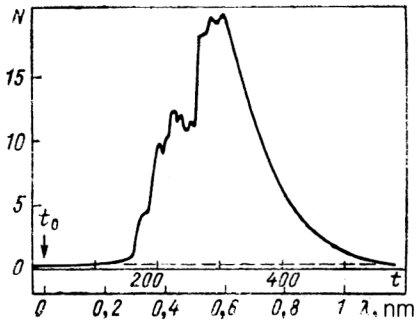

FIG. 4. Neutron-beam spectrum after a reflecting neutron guide tube and filtration. The width of the encoder channel is 128 μsec. On the vertical axis are the counts of a detector (a boron counter) of efficiency $\varepsilon(\lambda) = [1 - \exp(-0.07\lambda)]$, where λ is in units of 0.1 nm.

In the reactor mode for an average power 20 kW with burst duration 70 μsec and frequency 4 Hz the spectral density of the neutron flux at the location of the sample (35 m from the active zone of the reactor) was $3 \times 10^4/E^{0.96}$ eV^{-1}·cm^{-2}·sec^{-1} (the energy is in eV). In the booster mode for an average power 10 kW neutron pulses of duration 4.5 μsec were spaced at intervals of 100 Hz. Measurements of the asymmetry $\varepsilon^{F\text{-}B}$ on ^{11}Sn at epithermal neutron energies were made at the reactor IBR-2 at a mean power of 2 MW. The experiments were carried out in two neutron channels having maxima of the neutron spectra at different energies. An example of a time-of-flight spectrum characteristic of the evacuated ninth channel of the IBR-2 is shown in Fig. 3. The spectrum was obtained for a path length of 39 m by detection of the γ line of nickel with $E_\gamma = 9.0$ MeV by an NaI(Tl) detector. The width of the time-encoder channel was 64 μsec. Resonance, epithermal, and thermal neutrons are present in the spectrum. The duration of the power pulse of the IBR-2 of 215 μsec at a frequency of 5 Hz limits the neutron energy resolution $\simeq 5$ eV for this path length. Measurements using slower, cold neutrons were carried out for a path length of 24.6 m of the fifth channel. This channel had a curved reflecting neutron guide tube, which cleaned the beam well of epithermal and fast neutrons, and also γ quanta from the first power satellite in the range 1.05–1.1 nm. The satellites are periodic increases of the power of the pulsed reactor between the main bursts. After the installation of a 20-cm thick lead filter the background was eliminated at the cost of a 4-fold loss of intensity. An example of a time-of-flight spectrum of this beam obtained in the fifth channel of the IBR-2 is shown in Fig. 4.

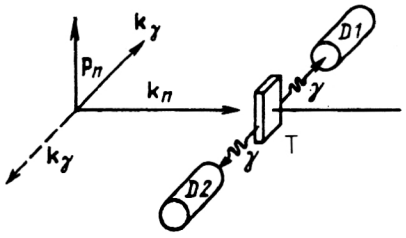

FIG. 5. Geometry of the experiments for measuring $\varepsilon^{L\text{-}R}$: T—target; D_1 and D_2—detectors. The rest is explained in the text.

The experimental scheme

The left—right asymmetry of the γ yields in the reactions ^{117}Sn(n,γ) and ^{113}Cd(n,γ) were measured by the time-of-flight method in the polarized neutron beam of the pulsed accelerator IBR-30. The experimental scheme is shown in Fig. 5. A polarized beam of resonance neutrons was created by passage through a polarized proton target[41–43] with a roughly 10-fold loss of intensity (Fig. 6). The target was a monocrystal of double lanthanum-magnesium nitrate [chemical formula $La_2Mg_3(NO_3)_{12}24H_2O$] of area 25 cm^2 and thickness 17 mm, in which the protons of the crystalized water were polarized by the "solid effect" (see, for example, Ref. 44). The magnetic induction at the target was 2.0 T and was directed perpendicular to the neutron beam. The neutron-polarization method is based on the fact that the cross section for neutron scattering on the proton in the triplet state (parallel spins) is about 3 times smaller than in the singlet state (antiparallel spins). As a result, the beam after passage through the proton target is polarized in the direction of the proton polarization. The value of the neutron polarization f_n was determined by measuring the transparency of the proton target[41] to neutrons of energy $E \simeq 1$ eV using two monitoring counters. One of them was placed in front of the proton target, and the other behind it. The value of the neutron polarization obtained in the experiments was 0.57 ± 0.02.

As can be seen from Fig. 6, the neutron polarization vector after passage through the proton target lies in the horizontal plane. To measure the left–right asymmetry the polarization vector should be perpendicular to the plane of the (n,γ) reaction. In our experiments this was the horizontal plane, which means that the polarization vector had to be vertical. This was done as follows (see Fig. 6): the polarized neutrons were passed through the gaps of two identical electromagnets with magnetic field $B \simeq 0.02$ T.

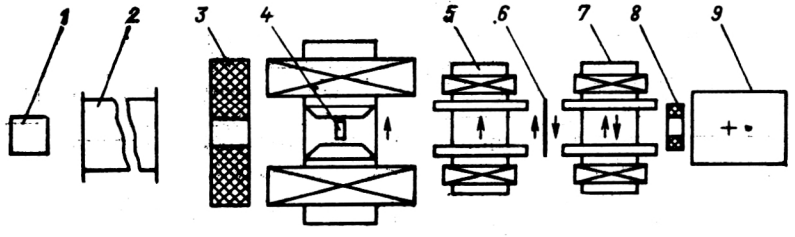

FIG. 6. Schematic view of the polarization setup: 1—reactor; 2—neutron guide tube; 3—shield; 4—proton target; 5, 7—electromagnets with horizontal magnetic field; 6—current foil; 8—collimator; 9—location of magnet with vertical field or solenoid. The arrows indicate the directions of the magnetic fields.

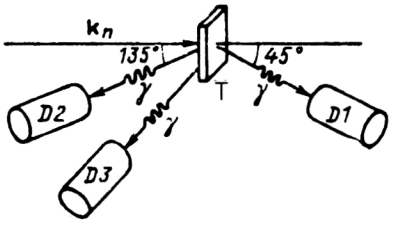

FIG. 7. Geometry of experiments for measuring $\varepsilon^{F\text{-}B}$: T—target; D_1, D_2, and D_3—detectors. The rest is explained in the text.

In the first of these magnets the field was parallel to the field at the target. The field of the second magnet could be switched on parallel or antiparallel to the field at the target. A foil with current generating a field $B \simeq 5 \times 10^{-3}$ T on its surface was placed between the electromagnets. On the side of the first electromagnet the field of the foil was parallel to the field inside it. If the fields in the electromagnets were parallel, then at the exit from the second magnet the direction of the neutron spin coincided with the field direction. If, however, the field in the second magnet was antiparallel to the field in the first, then a field gradient with alternating sign was created on the surface of the foil. This jump creates the conditions for nonadiabaticity of the transmission for the neutron spin; in other words, the neutron spin cannot be rotated along the field after the foil.

As a result, at the exit from the second magnet the initial spin direction is preserved, and the direction of the polarization vector relative to the field direction is reversed. For rotation of the polarization vector into the vertical plane after the second electromagnet another magnet was used. The field in it was of the same strength, but pointing in the perpendicular direction, and the direction was not changed during the experiment. In the gap between the second and third magnets the spin was adiabatically rotated by 90° into the vertical plane above or below, depending on the direction of the field in the second electromagnet. Therefore, the polarization vector was reversed. After the third electromagnet there was a magnet system with a guiding field for transporting the neutrons to the samples, which were located at a path length of 35 m. Replacement of the 90-degree rotation segment by a solenoid made it possible also to obtain longitudinally polarized neutrons for experiments on parity nonconservation (see Ref. 43 for details).

The forward–backward asymmetry of the γ yields $\varepsilon^{F\text{-}B}$ in the reactions $^{113}Cd(n,\gamma)$ and $^{117}Sn(n,\gamma)$ was measured by the time-of-flight method using the unpolarized beams of the reactor IBR-30 operating in the booster mode, and later at the IBR-2. The detector scheme in these experiments is shown in Fig. 7. Various path lengths from 38 to 56 m were used.

The detectors

The γ quanta of the direct transition with $E_\gamma = 9.04$ MeV in the reaction $^{113}Cd(n,\gamma)$ and with $E_\gamma = 9.32$ MeV in the reaction $^{117}Sn(n,\gamma)$ were recorded by NaI(Tl) detectors (with PM-49s) of diameter 200 mm and thickness 200 mm. The detectors were surrounded by a shield of lead and paraffin with boron. In addition, cassettes filled with $^6Li_2CO_3$ were placed all over the entire cylindrical surface right up to the crystal. A slab of paraffin with boron of thickness 10 cm was also installed in front of the collimator of diameter 160 mm at the entrance to the detector to eliminate direct detection of fast neutrons. The energy resolution of the crystals made it possible to distinguish the direct γ transitions of interest with $E_\gamma = 9.04$ MeV in ^{114}Cd and with $E_\gamma = 9.32$ MeV in ^{118}Sn from γ transitions to the first excited levels of the residual nuclei with $E_\gamma = 8.48$ MeV and $E_\gamma = 8.50$ MeV, respectively.

Examples of the amplitude γ spectra obtained on ^{117}Sn and ^{113}Cd are shown in Figs. 8 and 9. For the statis-

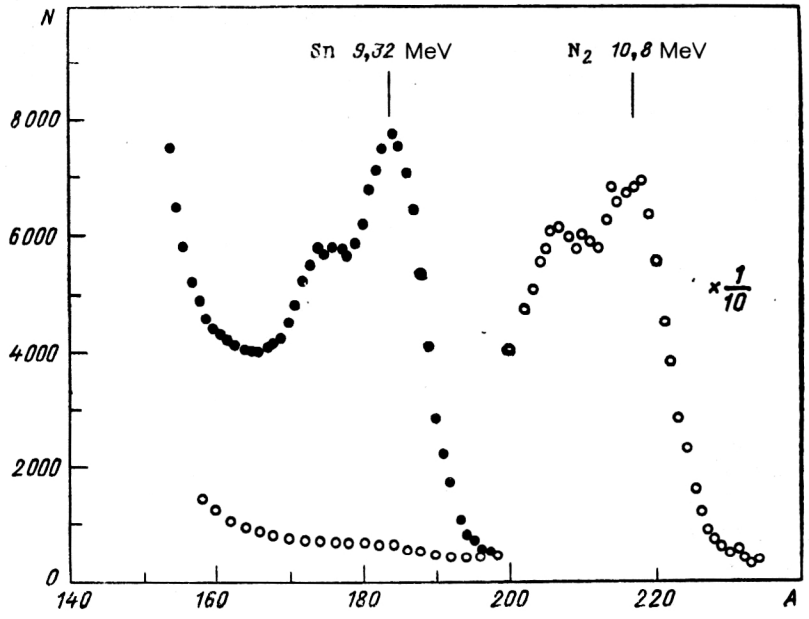

FIG. 8. Segments of the amplitude spectrum obtained with an NaI(Tl) detector after 20 hours of measurements for thermal neutrons: darkened points—spectrum of the ^{117}Sn sample; circles—background from the carbon sample; N_2—line from nitrogen in air; N—number of counts; A—channel number.

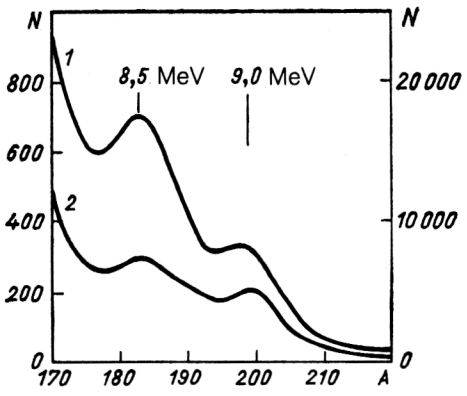

FIG. 9. Segments of the amplitude spectra of the ^{113}Cd sample obtained with an NaI(Tl) detector: 1—for neutrons with $E = 1$–4 eV, right-hand scale; 2—for neutrons in the resonance region $6.8 < E < 7.8$ eV, left-hand scale.

tical normalization of individual measurements we used a monitoring counter of the direct beam BF_3. The rather poor stability of the amplification of the NaI(Tl) detectors led to a systematic error, in addition to the geometrical asymmetry, in the measurement of $\varepsilon^{F\text{-}B}$. To estimate its value we made some additional measurements with a more stable Ge(Li) detector. The results of the measurements in the neutron energy range surrounding the entire thermal peak are shown in Fig. 10.

The detection electronics

Signals from the detectors were sent via the linear amplifiers by cable from the experimental hall of the IBR-30 or IBR-2 to the computational center of the Laboratory of Neutron Physics on the ACOR ("angular correlations") measurement module based on the SM-1300 computer (Fig. 11). The signals reached the input of the amplitude encoders (AC) (Ref. 45). The γ spectra were usually accumulated in 16 time windows (in 32 windows in the separate measurements using ^{113}Cd) by means of a digital window block (DWB) (Ref. 46) and held until they were written on the disk in an external 16-bit CAMAC 32 K memory. The electronics were triggered by start pulses with the same frequency as the reactor operation, which were fed to the input of the time encoder TCP-5. The marking of the time-of-flight spectrum into segments—time windows—was done by measurements of the time spectrum. After marking out the time spectrum the boundaries of the time windows and memory segments for different detectors were specified for the digital-window block. The time windows could have arbitrary duration and location. The width of a channel in microseconds was specified by the TCP-5 encoder. On-line data sorting was done by means of original FORUM programs (developed by T. Khrykina) and, later, CPN programs (Ref. 47). The programs allowed us to monitor the collected data and to do some very simple processing of them. The rest of the processing was done using the main PDP-11/70 computer of the Laboratory of Neutron Physics and the personal computer Pravets-16.

The background conditions

In the expressions of the preceding section for $\varepsilon^{L\text{-}R}$, $\varepsilon^{F\text{-}B}$, and ε_p, N or $N^{\pm}$ are understood to be the numbers of counts of γ quanta arising in a direct transition of the compound nucleus to the ground state. In any case, these numbers also contain counts from background γ quanta, which must be subtracted. From these expressions it is clear that incorrect inclusion of the background can lead, first, to a false effect (numerators) and, second, to an underestimate of the true size of the effect (denominators). It is therefore important to lower the background as much as possible and to make it as symmetric as possible for the two detector positions. Different components of the background play the dominant role, depending on the type of neutron guide tube (a curved reflecting one or simply an evacuated one) used. For example, a reflecting neutron guide tube cleans the beam well of fast neutrons and γ quanta from the active zone of the reactor. In any case, there is a constant background between reactor bursts, the background from the scattered neutrons and γ quanta from neutron capture by the equipment surrounding the detector. It can be suppressed by means of a lead shield and materials containing boron and ^{6}Li. The remaining constant background is measured in a time window far from the resonance between reactor bursts. The variable compo-

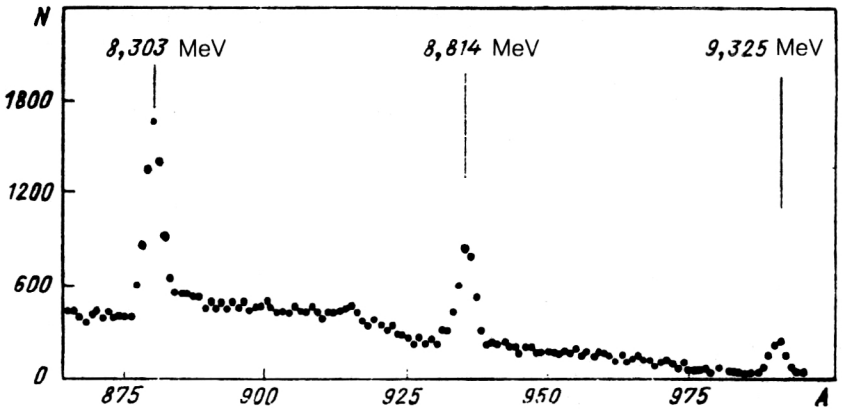

FIG. 10. γ spectrum of ^{117}Sn obtained at the IBR-2 with a Ge(Li) detector.

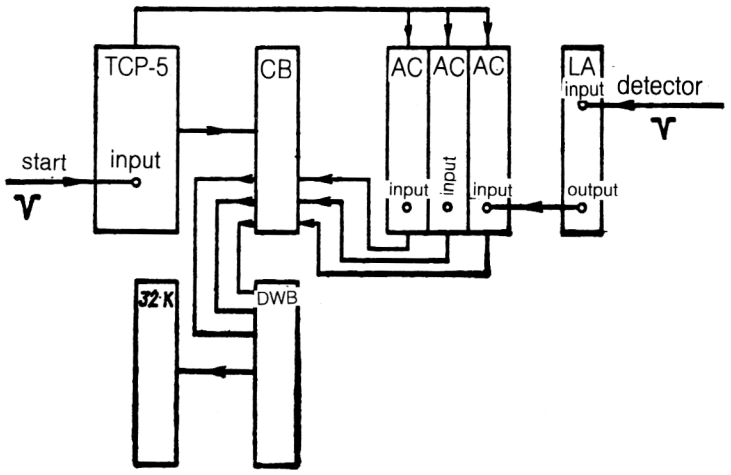

FIG. 11. Electronics scheme of the ACOR module for experiments to measure ε^{L-R} and ε^{F-B}: LA—linear amplifier; CB—block for controlling and encoding the detector number. The rest is explained in the text.

nent of the scattered-neutron background related to the burst can be measured by placing an equivalent carbon scatterer at the location of the sample. In the measurements with ^{113}Cd the background was determined using a resonance filter. The beam always contained a sample of metallic tantalum, which completely extracted, from the beam, neutrons of energies 4.3 and 10.3 eV. This made it possible to interpolate the background near the resonance studied at 7 eV. The time-of-flight spectrum obtained in the measurements with ^{113}Cd is shown in Fig. 12. In the measurements with ^{117}Sn the background was measured by alternately replacing the sample by an equivalent scatterer and a rhodium resonance filter.

The apparatus asymmetry

Inaccuracy in the geometrical alignment of the detectors, a difference in their efficiencies, and background all lead to systematic error in the determination of the magnitude of the effect. Allowance for the apparatus asymmetry is especially important in the measurement of small effects (when the estimated systematic error is of the order of the expected effect). As a control, the working sample was replaced by a sample which does not give the physical effect, so that the effect measured with the latter can be attributed completely to the apparatus asymmetry. It is important that the control sample give a γ transition with energy close to the one studied. For example, in the measurement of effects on ^{117}Sn in the direct γ transition with energy 9.32 MeV natural iron was used, which contains an isotope with a γ-transition energy of 9.3 MeV. The control can also be achieved using one of the softer γ lines of secondary transitions with high intensity I_γ, i.e., a large number of γ quanta per 100 entrapped neutrons, if such exist. Of course, such a line must not correspond to the physical effect. For example, for ^{117}Sn the γ transition with energy 1230 keV and $I_\gamma = 48 \pm 8$ can be used (Ref. 48). In this case the working and control measurements must be carried out in parallel, without changing the sample.

Instability of the amplification of the detector signal also leads to distortion of the magnitude of the effect, since it complicates the calibration. In this case errors can arise in finding the limits of the summation in the γ spectra in obtaining $N(E)$ or $N(\theta,E)$. For example, in our experiments with ^{117}Sn a shift of the energy summation interval in the spectrum of one detector relative to the other by a single channel ($\simeq$43 keV) led to a false effect $\varepsilon \simeq 0.01$ at a working threshold of 8.5 MeV. It is especially important to eliminate this error in the measurement of small effects. Therefore, even when stabilization of the amplification occurs in the system it is useful to make measurements in the

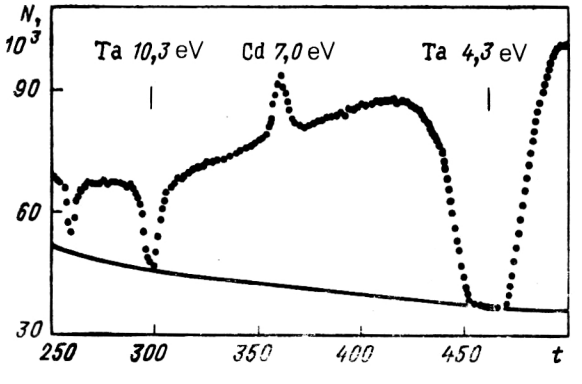

FIG. 12. Time-of-flight spectrum obtained using a tantalum filter for the ^{113}Cd sample. The detection threshold is 2 MeV, and the width of the encoder channel is 4 μsec.

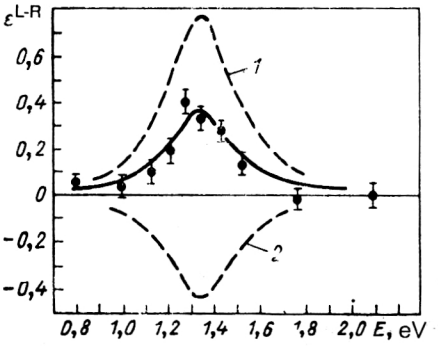

FIG. 13. Asymmetry ε^{L-R} for ^{117}Sn in the vicinity in the resonance at 1.33 eV. The smooth curves were calculated; see Sec. 5 for the explanation.

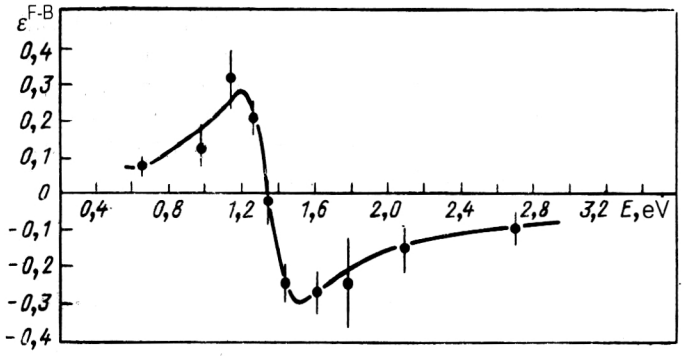

FIG. 14. Asymmetry ε^{F-B} for ^{117}Sn near the resonance at 1.33 eV.

thermal spectrum with the more stable Ge(Li) detector to use it to normalize the results of the measurements with the NaI(Tl) detector in the epithermal region.

In measurements of ε^{L-R} by a single detector it was practically unnecessary to take into account the apparatus asymmetry, since it was not necessary to change the position relative to the beam, and the variations of the conditions in the rapid reversal of the polarization vector had identical effects on the γ spectra for the two polarization directions. However, measures were taken to screen the scintillation detector from the channel magnetic field, which affected the PM amplification coefficient.

Conversely, measurements of ε^{L-R} required accurate inclusion of the false asymmetry. In our experiments both with ^{113}Cd and with ^{117}Sn the apparatus asymmetry was measured using a disk of ordinary iron at the location of the sample. The iron does not produce the physical effects ε^{L-R} and ε^{F-B}, so that the asymmetry obtained in the direct γ transition with $E_\gamma = 9.3$ MeV corresponds entirely to the apparatus asymmetry. However, it is possible to have an error in the sample replacement, and, moreover, measurement of the false asymmetry takes time. Therefore, in the experiments with ^{117}Sn using the IBR-2 we monitored the apparatus asymmetry also using the γ transition with $E_\gamma = 1230$ keV to the ground state of ^{118}Sn. The high intensity of this transition allowed us to simultaneously normalize the spectra in the intensity. The measurements were made with a Ge(Li) detector.

The data processing

The measurements of ε^{L-R} and ε^{F-B} at the IBR-30 were done near the p-wave resonances with $E_0 = 7$ eV for ^{113}Cd and $E_0 = 1.33$ eV for ^{117}Sn. In addition, for ^{117}Sn in the IBR-2 reactor we measured ε^{F-B} in the neutron energy range 0.005–3 eV (Ref. 49). At the IBR-30 reactor measurements of ε^{L-R} were made using metallic samples of cadmium (95% ^{113}Cd) and tin (91% ^{117}Sn) for path lengths of 52 and 58 m, respectively. The experiments to measure ε^{L-R} were carried out on a path length of 35 m. To record the γ quanta of the direct transitions with $E_\gamma = 9.04$ MeV in ^{114}Cd and $E_\gamma = 9.32$ MeV in ^{118}Sn at different times we used one, two, or three LaI(Tl) detectors. The detectors were located at angles of 45, 90, and 135° or 55, 90, and 125°. The angles 55 and 125° were chosen because for $\theta = 54.7°$ and $\theta = 125.3°$, as seen from the expression for the differential cross section $\sigma(\theta,\varphi,E)$, $P_2(\cos\theta)$ vanishes, and this simplifies the expressions.

The initial data for processing were the 16 (or 32) amplitude γ spectra. They included the segments of interest of the time-of-flight spectrum for calculating the left–right and forward–backward effects and the background segments. In addition, there were the analogous γ spectra obtained with the iron and carbon samples. In the processing we first normalized all the γ spectra to the same measurement time. In the cases where the asymmetry ε^{F-B} was measured by only a single detector, for the normalization we used the data of the beam-intensity monitor. Then we subtracted the backgrounds, determined by the procedure described above, from all the needed γ spectra. After this the asymmetry ε^{L-R} or ε^{F-B} was calculated using the expressions given above. For this we first did the energy calibration of the amplitude spectra, and then we took the sums in the intervals of the needed γ lines. Usually intervals of 8.5–9.7 MeV were selected for the spectra from all the detectors. In the measurement of ε^{F-B} the same procedure was performed for the γ spectra obtained with iron in

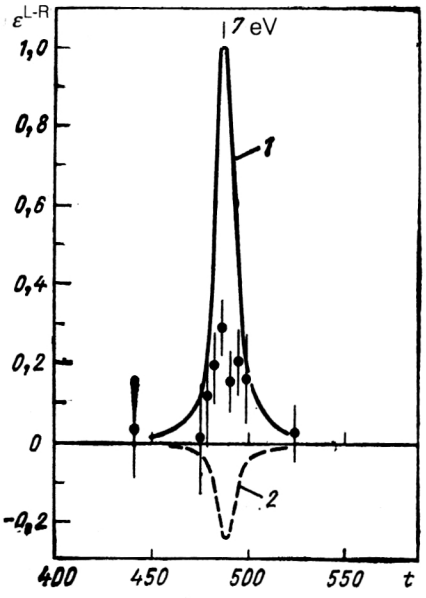

FIG. 15. Asymmetry ε^{L-R} for ^{113}Cd: 1 and 2 are the calculated curves (explained in Sec. 5).

order to take into account the apparatus asymmetry. In processing the results of the measurements of $\varepsilon^{F\text{-}B}(^{117}Sn)$ at the IBR-2 the normalization of the individual measurements made at different angles and the inclusion of the apparatus asymmetry were done using the soft γ transition with $E_\gamma = 1230$ keV to the ground state of ^{118}Sn and using the measurements with the Ge(Li) detector and time window encompassing the entire thermal spectrum.

The intensities of direct $M1$ transitions in thermal-neutron capture in ^{118}Sn obtained in these measurements[48] are given below for different values of the γ energy E_γ corresponding to the final-level energies:

$E_{\gamma i}$, keV	9325	8095	7565	7269 7281	6996	6925	6414
E_f, keV	0	1230	1760	2056 2044	2329	2400	2911
J_f^π	0^+	2^+	0^+	$0^+(2^+)$	$1^+(2^+)$	(2^+)	(2^+)
I_f	3.0 ± 0.5	0.36 ± 0.1	$\leqslant 0.1$	0.60 ± 0.15	0.4 ± 0.1	$\leqslant 0.1$	1.27 ± 0.2

Here the probable values are given in parentheses.

The results of the measurememts of $\varepsilon^{L\text{-}R}$ and $\varepsilon^{F\text{-}B}$ for ^{117}Sn are shown in Figs. 13 and 14, and for ^{113}Cd in Figs. 15 and 16. In addition to the values of $\varepsilon^{L\text{-}R}$ and $\varepsilon^{F\text{-}B}$ for tin and cadmium, in the processing we obtained the values of the angular asymmetry of the p-wave part of the cross section $\varepsilon_p^a(\theta)$. For ^{117}Sn, ε_p^a was determined for the angle $\theta = 45°$, and for ^{113}Cd it was found for $\theta = 55°$. For tin the γ spectra at different angles were normalized to the same number of counts in the thermal energy region, where the angular distribution was assumed to be isotropic. The time-of-flight spectrum thus obtained for ^{117}Sn is shown in Fig. 17. We note that Fig. 17 is constructed from the data obtained at the IBR-2, and in analyzing it, it is necessary to take into consideration the fact that the time resolution of the IBR-2 spectrometer decreases the observed peak γ yield by a factor of 2.

For ^{113}Cd the thermal spectrum was absent, and therefore we normalized to the s-wave substrate, assuming that it is isotropic. An example of the corresponding spectrum is given in Fig. 18. The areas under the p-resonance curves $N(90°)$ and $[N(\theta) + N(180° - \theta)]/2$ were calculated over the smooth s-wave background for both of the resulting spectra.

The last stage of the processing was the inclusion of the Doppler effect and the resolution function. For these calculations we used the values of the p-resonance parameters for ^{117}Sn and ^{113}Cd from Ref. 50. They are given in Table I (the error in the last significant digit is given in parentheses).

For the effects $\varepsilon^{L\text{-}R}$ and $\varepsilon^{F\text{-}B}$ in tin the Doppler shift

$$\Delta = (kT_{\text{eff}}E_0/A)^{1/2}$$

is small ($\simeq 0.035$ eV for $\Gamma = 0.18$ eV) and is of no practical importance. For ^{113}Cd, $\Delta = 0.08$ eV for $\Gamma = 0.16$ eV, so that it is not necessary to include the Doppler effect. In this case the theoretical and experimental data were compared as follows. First, having calculated the tabulated value of the Doppler function ψ_Δ at the center of the resonance, from the experimental time-of-flight spectrum for $\theta = 90°$ we reconstructed the theoretical curve of the cross section near the p resonance. Then, using this curve to find the terms a_0, a_1, and a_2 in the equation for $\sigma(\theta,\varphi,E)$, we constructed the theoretical curves for the cross sections in the p-resonance region at the angles $\theta = 55°$ and $\theta = 125°$ for different sets of x and y. These cross sections were folded in with the exact Doppler function of the neutron energy distribution

$$f(E,E') = (A/4\pi kT_{\text{eff}})^{1/2} \exp\{-A[(E')^{1/2} - E^{1/2}]\},$$

which actually reduced to a Gaussian distribution of the form

$$f(E,E') = (1/\Delta\sqrt{\pi}) \exp[-(E-E)^2/\Delta^2].$$

Finally, Eq. (14) was used to obtain $\varepsilon^{F\text{-}B}$.

The optimal set of parameters, which is discussed in the following section, gave the curve shown in Fig. 16. For $\varepsilon_p^a(\theta)$ using ^{113}Cd we obtained the value $\varepsilon_p^a(55°) = 0.90 \pm 0.15$. The error is systematic and is related to the uncertainty in the background level, which was taken into account in the normalization to the s-wave component of the cross section. For the ratios of the areas under the p-resonance curves of ^{117}Sn at different angles $N(90°)/[N(45° + 135°)/2]$ the value $\varepsilon_p^a = 1.18 \pm 0.12$ was found in recent measurements,[49] where the error is due to the uncertainty in the level of the substrate under the p reso-

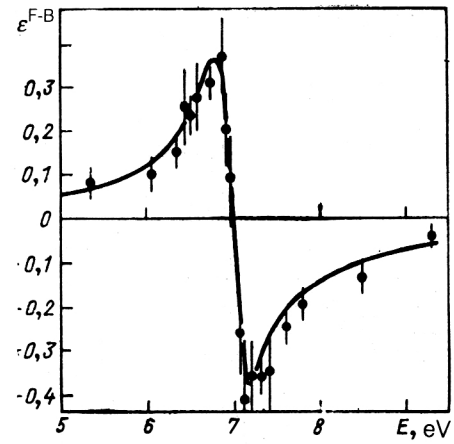

FIG. 16. Asymmetry $\varepsilon^{F\text{-}B}$ for ^{113}Cd near the resonance at 7 eV.

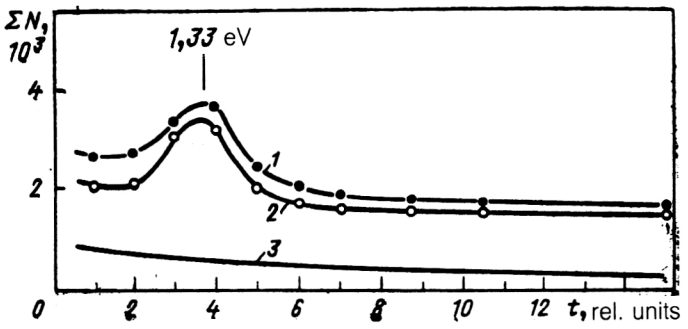

FIG. 17. Time-of-flight spectrum of the ^{117}Sn sample in the resonance region (ΣN is the number of counts of the amplitude encoder in the interval E_γ = 8.5–9.5 MeV for the width of the time window equal to 192 μsec): 1—the angle 90°; 2—the angle (45° + 125°)/2; 3—background for the angle 90°.

nance. The authors of the more recent study of Ref. 52 gave a different result: $\varepsilon_p^a = 1.63 \pm 0.14$.

5. RESULTS OF (n,γ) EXPERIMENTS

Tin

The amplitudes of the neutron partial widths $G_{jn}^{1/2}$ can be obtained in the form of two sets by measuring any asymmetry ($\varepsilon^{F\text{-}B}$, or $\varepsilon^{L\text{-}R}$, or ε_p^a), the description of which involves the reduced amplitudes $x = (\Gamma_{n1/2}/\Gamma_n)^{1/2}$ and $y = (\Gamma_{n3/2}/\Gamma_n)^{1/2}$, and using the fact that $x^2 + y^2 = 1$. The values of x and y were first obtained in an experiment to measure $\varepsilon^{L\text{-}R}$ on ^{117}Sn (Ref. 51). The corresponding results are shown in Figs. 19a and 19b. The smooth curve describing the data for $\varepsilon^{L\text{-}R}$ on ^{117}Sn corresponds to a least-squares fit. However, one measurement is not enough for determining the sign of the amplitudes. The point is that x and y enter into all the expressions quadratically. Other experiments were needed to choose the signs of x and y, and when they were done, the situation became dramatic. The results of the subsequent measurements of $\varepsilon^{F\text{-}B}$ on ^{117}Sn were not consistent with the data for $\varepsilon^{L\text{-}R}$, and the data for both of these cases were inconsistent with ε_p^a. In Figs. 13 and 14 we give the data of Ref. 52, where this discrepancy was first discovered.

The values of x and y obtained by a least-squares fit for each of the effects $\varepsilon^{L\text{-}R}$ and $\varepsilon^{F\text{-}B}$ with the parameters $t_{90°}^2 = 3.0 \pm 0.3$ and $t_{45°}^2 = 1.83 \pm 0.18$ turned out to be inconsistent: for example, if one attempts to describe the data for $\varepsilon^{L\text{-}R}$ using the sets of values of x and y obtained for $\varepsilon^{F\text{-}B}$ (smooth curve in Fig. 14), then one of the curves lies much higher than the experimental data (curve 1 in Fig. 13), and the second, although it does give an adequate quantitative description of the data, gives the opposite sign of the effect (curve 2 in Fig. 13). For $\varepsilon_p^a(45°)$ the value 1.63 ± 0.14 was obtained in the same experiment.[52] We note that the maximum value of $\varepsilon^{L\text{-}R}$ in Fig. 19 is about 0.1 smaller than in Fig. 13, since a smaller value for $t_{90°}^2$ corresponding to $\varepsilon_p^a = 1.2$ was obtained in Ref. 51.

Of course, this situation led to doubts about the correctness of the expressions for the asymmetries, the correctness of the processing algorithm, and the value of the neutron polarization. However, careful study did not reveal any errors. An additional series of experiments was then carried out at the IBR-2 (Ref. 49), in which the asymmetry $\varepsilon^{F\text{-}B}$ on ^{117}Sn was measured at energies below the p resonance, where the background conditions are considerably better. If the result obtained earlier for $\varepsilon^{F\text{-}B}$ near the resonance is correct, the discrepancy between experiment and theory should also appear here. The results of these measurements are shown in Figs. 20 and 21 (Ref. 49), where the theoretical curves were calculated in the following manner. The value $\varepsilon_{max}^{L\text{-}R} = 0.35$ at the resonance $E_0 = 1.33$ eV (Ref. 52) and the value $t_{90°}^2 = 2.16$ obtained by multiplication of the newly measured value $\varepsilon_p^a = 1.18 \pm 0.12$ and the parameter $t_{45°}^2 = 1.83$ were used. According to Eq. (23), they led to two sets of x and y (Ref. 49):

$$x = 0.528 \pm 0.037;\ y = -0.813 \pm 0.027; \tag{29}$$

$$x = 0.009 \pm 0.009;\ y = +0.999 \pm 0.021. \tag{30}$$

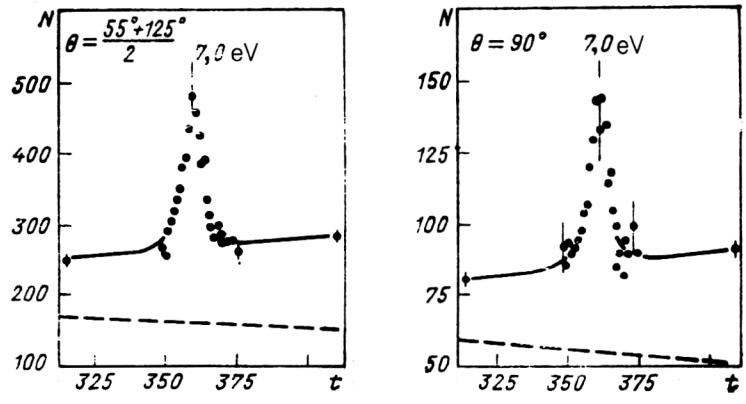

FIG. 18. Time-of-flight spectrum obtained in the reaction ^{113}Cd(n,γ) for various angles. N is the number of detector counts in the amplitude interval 8.7–9.5 MeV, and the dashed line is the background level for an encoder channel width of 4 μsec.

TABLE I. Parameters of the p resonances of ^{117}Sn and ^{113}Cd.

Nuclide	E_p, eV	J	$g\Gamma_n$, 10^{-7} eV	Γ, meV	$E_{\gamma i}$, MeV	$\Gamma_{\gamma 0}$, meV	Γ_{n1}/Γ_n
^{113}Cd	7,0	1	3,1(3)	160(20)	9,04	4,5(9)	0,84(7)
^{117}Sn	1,33	1	1,66(20)	180(18)	9,32	1,2(3)	0,18(8)

We note that these two sets of x and y are close to the values from Ref. 51. Then with these sets Eq. (22) was used to find the calculated curves for $\varepsilon^{F\text{-}B}(E)$. In Figs. 20 and 21 the curves labeled 1 are for the set (29), and those labeled 2 are for the set (30). We note that the theoretical value of $\varepsilon^{F\text{-}B}$ has not been corrected by the resolution function. With the correction its maximum value turns out to be slightly smaller, but the discrepancy remains. Beyond the region $E_0 = 0.3$ eV the effect of the resolution function is already completely insignificant, so that the comparison of the experimental data with the theory is completely correct. We see that in the vicinity of the resonance the discrepancy is large, as before, but it decreases in going to thermal energies.

Cadmium

The results for $\varepsilon^{L\text{-}R}$ and $\varepsilon^{F\text{-}B}$ on ^{113}Cd from Ref. 53 are shown in Figs. 15 and 16. Curves 1 and 2 in Fig. 15 were also obtained from the two sets of x and y for $\varepsilon^{F\text{-}B}$ at $\theta = 54.7°$ and $\theta = 125.3°$. We recall that the parameter $t^2_{90°} = 2.27$ was used for the fit to $\varepsilon^{L\text{-}R}$, and the parameter $t^2_{55°} = 2.5 \pm 0.3$ was used for $\varepsilon^{F\text{-}B}$. The following two sets of x and y were obtained from $\varepsilon^{F\text{-}B}$ in Ref. 53:

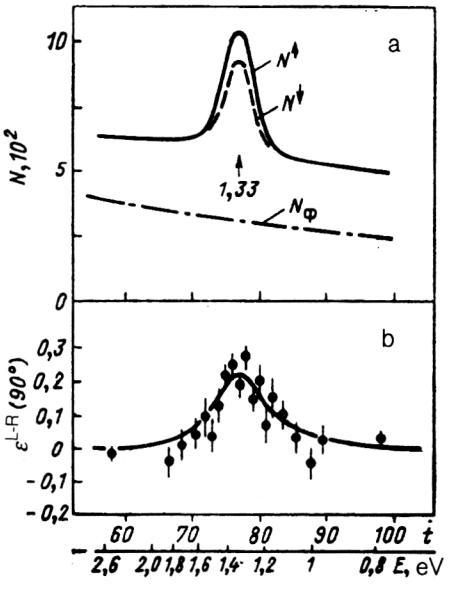

FIG. 19. Results of Ref. 51 for ^{117}Sn: a—time-of-flight spectra in the vicinity of the p resonance at 1.33 eV for two directions of the polarization vector (width of the encoding channel equal to 32 μsec); b—the asymmetry $\varepsilon^{L\text{-}R}$.

$$x = 0.975;\ y = 0.222; \tag{31}$$

$$x = 0.100;\ y = -0.995. \tag{32}$$

The set (31) corresponds to curve 1 in Fig. 15, and the set (32) to curve 2.

It is obviously premature to view these values of x and y, both for ^{113}Cd and for ^{117}Sn, as the true values of the partial amplitudes, since there is no agreement between the results of the experiments.

There is another clearer representation of the results of the parameter determination: in graphical form. This is done for ^{113}Cd in Fig. 22. For all three values $\varepsilon^{L\text{-}R}$, $\varepsilon^{F\text{-}B}$, and ε^a_p curves are constructed with the known parameters t^2_θ for all possible x and y. The dashed lines show the corresponding errors. Since $x^2 + y^2 = 1$, all three curves should intersect within the experimental error near one point on the circle. This did not occur, which means that the results are inconsistent. The dot–dash line corresponds to the case where an overall minus sign is introduced on the right-hand side of (23) or the sign of the beam polarization is changed. This is given to stimulate further searches. We also note that ε^a_p has the largest error corridor, and decreasing it is an important but difficult experimental problem. A similar graphical illustration of the results for ^{117}Sn is given in Ref. 52.

The situation is therefore unclear. Since no serious errors were found in the experimental work or in the data processing, it is logical to seek a physical reason for the discrepancy. We note that the system of equations for $\varepsilon^{L\text{-}R}$ and $\varepsilon^{F\text{-}B}$ together with $x^2 + y^2 = 1$ and the equation for the asymmetry of the p-wave part of the cross section $\varepsilon^{F\text{-}B}$ is overdetermined in x and y. The inclusion of another unknown parameter would obviously permit the description of the available data on $\varepsilon^{F\text{-}B}$ and $\varepsilon^{L\text{-}R}$. Physically, this parameter might correspond to the contribution of the nonresonance d-capture amplitude in the vicinity of the p resonance. The formal inclusion of the d wave leads, as shown for the example of the s representation, to additional terms in Eqs. (28). The presence of the d wave can be established experimentally by measuring the anisotropy ε^a_d in the epithermal range of neutron energies.

Below we give the values of ε^a_d for ^{117}Sn at several neutron energies for $f_d/f_s = -0.6$ near the resonance $E_0 = 1.33$ eV:

E, eV	1.33	0.80	0.50	0.20
ε^a_d	1.48	1.29	1.18	1.06

The value of f_d/f_s was obtained by numerical solution of the system of equations for $\varepsilon^{L\text{-}R}$ and $\varepsilon^{F\text{-}B}$ and Eq. (25) at the resonance, including the d wave.

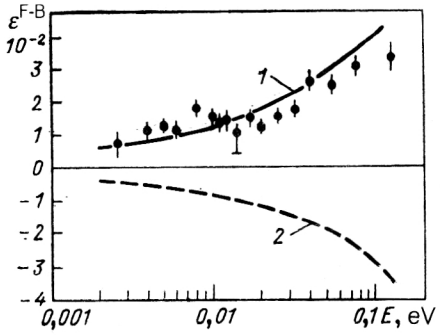

FIG. 20. Asymmetry ε^{F-B} on ^{117}Sn at neutron energies below 0.1 eV: 1, 2 are calculated curves explained in Sec. 5.

However, to describe the results the value of this background amplitude according to the estimate in Ref. 54 must correspond to a roughly 25% s-wave partial differential cross section for radiative capture followed by an $M1$ γ transition. In the absolute expression for ^{117}Sn this amounts to about 10^{-28} cm^2/sr for $E = E_0$. At low neutron energies this is a very large cross section, and so the appearance of d capture is doubtful. None of the studies described provides a direct experimental check of the contribution of this mechanism, since the measurement technique used is based on the assumption of an isotropic γ distribution at energies away from the resonance.

Another physical mechanism which might affect the discrepancy between the experimental results and the theoretical predictions has been proposed by Zaretskiĭ and Sirotkin.[30] They noted that a detector with a resolution of about 0.5 MeV could register the hard component of a two-quantum cascade consisting of a primary soft photon of energy of about 0.5 MeV followed by a transition to the ground state. This process increases the coefficient a_0, but does not affect the coefficients a_1 and b_1, since the hard quanta in the cascade come from intermediate states which are not mixed in parity. The total contribution of two-quantum cascades to the asymmetries ε^{L-R} and ε^{F-B}, enhanced by the valence mechanism, can reach 10% according to the estimate of Ref. 30. However, the discrepancy between the results in the vicinity of the p resonance could be explained by only a 50% contribution of this process. This mechanism can be tested experimentally using a Ge(Li) detector of high resolution.

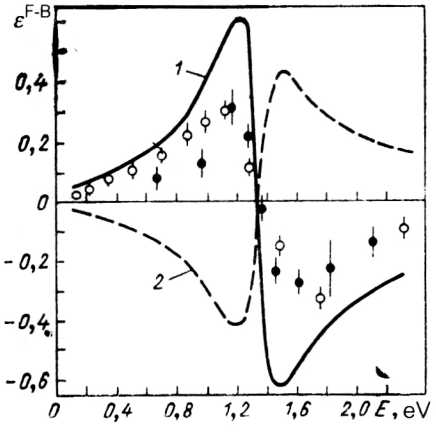

FIG. 21. Asymmetry ε^{F-B} on ^{117}Sn at neutron energies 0.1–2.5 eV: 1, 2 are calculated curves explained in Sec. 5, the darkened points are from Ref. 52, and the circles are from Ref. 49.

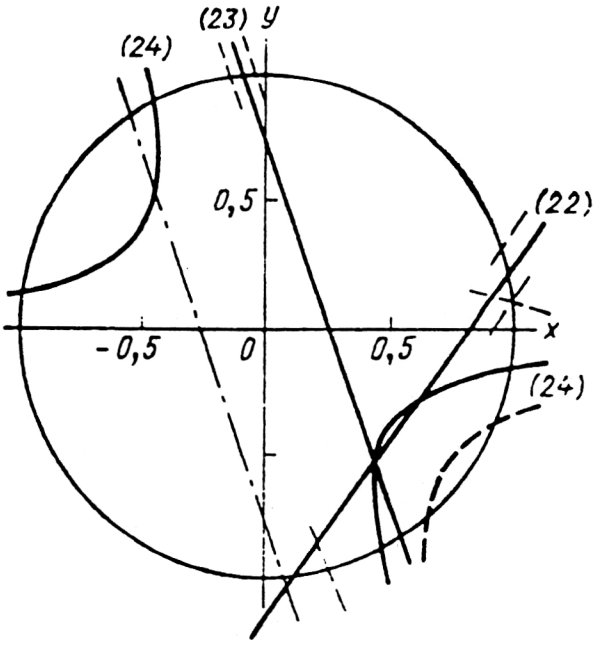

FIG. 22. The dependence $y(x)$ for ^{113}Cd obtained from Eqs. (22)–(24). The numbers in parentheses near the curves correspond to the equation numbers.

CONCLUSION

Analysis of the available information leads to the conclusion that the resonance model with two spin channels may be inadequate for describing the real process, resulting in the discrepancies found. Conclusions about more serious consequences for the theory are premature.

Actually, the quantum-mechanical conservation laws impose constraints on the number of independent reaction amplitudes.[55] It can be shown that the problem considered with $I = 1/2$, $I_f = 0$, and $J = 1$ is characterized by four independent amplitudes. Even if the d wave is neglected, there still remain three amplitudes, i.e., five real parameters: three moduli and two relative phases, which require for their experimental, model-independent determination no less than five independent equations and the corresponding number of experiments. Actually, not five but seven equations are needed, since the physical observables are non-single-valued quadratic functions of the amplitudes and their phases.

The experiments that we have analyzed ensure only three independent equations. A model-independent analy-

sis of them is impossible, so that there is not yet any basis for fundamental conclusions.

The additional equations needed can be provided by experiments in which the polarizations of all the particles are measured for two spatial directions: for example, in the reaction plane and in a plane perpendicular to it. The corresponding theoretical calculations also need to be carried out. The foundation was laid by the work of Efimov,[29] in which the linear polarization of the quanta emitted in the capture of a polarized neutron was calculated, and it was shown that this gives a new independent equation for determining the channel-mixing parameter x_s. Obviously, a complete experiment must include measurement of not only the linear polarization of the quanta, but also the angular correlations on polarized nuclei. It is also desirable to extend the set of investigated nuclei and γ transitions (see the tabulated data for I_f), and to make measurements with high resolution in the γ energy.

The authors would like to thank V. P. Alfimenkov, L. B. Pikel'ner, and A. P. Sirotin for solving a number of organizational and technical problems in carrying out the experiments and for fruitful discussions. Discussions of the theoretical questions with V. N. Efimov, V. I. Furman, O. P. Sushkov, G. Mitchel and J. Vanhoy greatly aided our understanding of the problem, and we are deeply grateful to them.

[1] E. P. Wigner, *Gruppentheorie und ihre Anwendung auf die Quantenmechanik der Atmospektren* (Vieweg, Braunschweig, 1931); *Group Theory and Its Application to Quantum Mechanics of Atomic Spectra* (Academic, New York, 1959).
[2] G. Racah, Phys. Rev. **62**, 438 (1942).
[3] G. Racah, Phys. Rev. **63**, 367 (1943).
[4] U. Fano, Phys. Rev. **90**, 577 (1953).
[5] F. Coester and J. M. Jauch, Helv. Phys. Acta **36**, 3 (1953).
[6] L. C. Biedenharn and M. E. Rose, Rev. Mod. Phys. **25**, 729 (1953).
[7] A. Simon, Phys. Rev. **92**, 1050 (1953).
[8] M. I. Shirokov, Zh. Eksp. Teor. Fiz. **32**, 1022 (1957) [Sov. Phys. JETP **5**, 835 (1957)]; **33**, 975 (1957) [**6**, 748 (1958)].
[9] R. Huby, Proc. Phys. Soc. London **72**, 97 (1958).
[10] L. J. Goldfarb, in *Nuclear Reactions*, edited by P. M. Endt and M. Demeur (North-Holland, Amsterdam, 1959), Vol. 1, p. 159.
[11] A. M. Baldin, V. I. Gol'danskiĭ, and I. L. Rozental', *Kinematics of Nuclear Reactions* (Oxford University, London, 1961) [Russian original, Fizmatgiz, Moscow, 1959].
[12] A. J. Ferguson, *Angular Correlation Methods in Gamma-Ray Spectroscopy* (North-Holland, Amsterdam, 1965).
[13] R. D. Gill, *Gamma-Ray Angular Correlations* (Academic, New York, 1975).
[14] Yu. G. Abov, P. A. Krupchitsky, and Yu. A. Oratovsky, Phys. Lett. **12**, 25 (1964).
[15] P. A. Krupchitsky, *Fundamental Research with Polarized Slow Neutrons* (Springer-Verlag, New York, 1987) [Russian original, Énergoatomizdat, Moscow, 1985].
[16] V. P. Alfimenkov, S. B. Borzakov, Vo Van Thuan *et al.*, Pis'ma Zh. Eksp. Teor. Fiz. **34**, 308 (1981) [JETP Lett. **34**, 295 (1981)].
[17] V. P. Alfimenkov, Usp. Fiz. Nauk **144**, 361 (1984) [Sov. Phys. Usp. **27**, 797 (1984)].
[18] S. A. Biryukov, L. N. Bondarenko, S. V. Zhukov *et al.*, Yad. Fiz. **45**, 1511 (1987) [Sov. J. Nucl. Phys. **45**, 937 (1987)].
[19] Y. Masuda, T. Adachi, A. Masaike *et al.*, Nucl. Phys. **A478**, 737c (1988).
[20] J. D. Bowman, C. D. Bowman, J. E. Bush *et al.*, Phys. Rev. Lett. **65**, 1192 (1990).
[21] P. K. Kabir, in *Tests of Time Reversal Invariance in Neutron Physics*, edited by N. R. Roberson, C. R. Gould, and J. D. Bowman (World Scientific, Singapore, 1987), p. 100.
[22] G. E. Mitchel, E. G. Bilpuch, J. F. Shriner *et al.*, Phys. Rep. **117**, 3 (1985).
[23] R. O. Nelson, E. G. Bilpuch, and G. E. Mitchel, Nucl. Instrum. Methods **A236**, 128 (1985).
[24] G. S. Samosvat, Fiz. Elem. Chastits At. Yadra **17**, 713 (1986) [Sov. J. Part. Nucl. **17**, 313 (1986)].
[25] C. M. McGullagh, M. J. Kenny, R. E. Chrien *et al.*, Phys. Rev. C **19**, 539 (1979).
[26] R. G. Seyler and H. R. Weller, Phys. Rev. C **30**, 1146 (1984); **20**, 453 (1979).
[27] O. P. Sushkov and V. V. Flambaum, Nucl. Phys. **A435**, 352 (1985).
[28] J. R. Vanhoy, E. G. Bilpuch, J. F. Shriner *et al.*, Z. Phys. A **331**, 1 (1988).
[29] V. N. Efimov, Communications R4-88-848, R4-88-528, JINR, Dubna (1988) [in Russian].
[30] D. F. Zaretskiĭ and V. K. Sirotkin, Yad. Fiz. **52**, 395 (1990) [Sov. J. Nucl. Phys. **52**, 253 (1990)].
[31] R. W. Carr and J. E. E. Baglin, Nucl. Data Tables A **10**, 143 (1971).
[32] R. M. Laszewski and R. J. Holt, At. Data Nucl. Data Tables **19**, 305 (1977); **23**, 97 (1979).
[33] S. Devons and M. G. Hime, Proc. R. Soc. London **199**, 73 (1949).
[34] D. Y. Schlueter, R. W. Krone, F. W. Prosser *et al.*, Nucl. Phys. **A58**, 254 (1964).
[35] J. Ulbricht, W. Arnold, H. Berg *et al.*, Nucl. Phys. **A287**, 220 (1977).
[36] F. C. Barker and N. Ferdous, J. Phys. G **7**, 1239 (1981).
[37] K. A. Snover, B. G. Ikossi, E. G. Adelberger *et al.*, Phys. Rev. Lett. **44**, 927 (1980).
[38] J. C. Brown, R. G. Seyler, T. L. Tsin *et al.*, Phys. Rev. C **31**, 1607 (1985).
[39] H. R. Weller, D. R. Tilley, G. Feldman *et al.*, TUNL Annual Report, Vol. 26, p. 36, 1987.
[40] T. R. Wang, W. Haeberli, S. W. Wissink *et al.*, Phys. Rev. C **37**, 2301 (1988).
[41] V. I. Lushchikov, Yu. V. Taran, and F. L. Shapiro, Yad. Fiz. **10**, 1178 (1969) [Sov. J. Nucl. Phys. **10**, 669 (1970)].
[42] V. P. Alfimenkov, A. V. Androsov, A. I. Ivanenko *et al.*, Communication 13-9396, JINR, Dubna (1975) [in Russian].
[43] V. P. Alfimenkov, S. B. Borzakov, Vo Van Thuan *et al.*, Nucl. Phys. **A398**, 93 (1983).
[44] O. V. Lounasmaa, *Experimental Principles and Methods Below One Degree Kelvin* (Academic, New York, 1974) [Russian transl., Mir, Moscow, 1977].
[45] A. A. Bogdzel', M. Z. Ishmukhametov, and V. G. Tishin, Communication 10-8641, JINR, Dubna (1975) [in Russian].
[46] V. A. Vagov, V. E. Novozhilov, and A. P. Sirotin, Communication R10-86-562, JINR, Dubna (1986) [in Russian].
[47] D. I. Lyapin *et al.*, Communication R13-89-352, JINR, Dubna (1989) [in Russian].
[48] V. R. Skoĭ and É. I. Sharapov, Communication R3-90-126, JINR, Dubna (1990) [in Russian].
[49] D. I. Lyapin, I. M. Salamatin, A. P. Sirotin *et al.*, Communication R3-90-125, JINR, Dubna (1990) [in Russian].
[50] V. P. Alfimenkov, S. B. Borzakov, and Yu. D. Mareev, Communication R3-87-117, JINR, Dubna (1987) [in Russian].
[51] V. P. Alfimenkov, S. B. Borzakov, and Vo Van Thuan, Pis'ma Zh. Eksp. Teor. Fiz. **39**, 346 (1984) [JETP Lett. **39**, 416 (1984)].
[52] V. P. Alfimenkov, S. B. Borzakov, and Yu. D. Mareev, Brief Communication No. 10-85, JINR, Dubna (1985), p. 19 [in Russian].
[53] V. P. Alfimenkov, S. B. Borzakov, Yu. D. Mareev *et al.*, Yad. Fiz. **52**, 927 (1990) [Sov. J. Nucl. Phys. **52**, 589 (1990)].
[54] É. I. Sharapov, in *Proc. of the 5th Intern. School on Neutron Physics*, D3, 4, 17, 86-747, JINR, Dubna, 1987, p. 113 [in Russian].
[55] R. G. Goldstein and M. J. Moravchik, Nucl. Instrum. Methods **A240**, 43 (1985).

Translated by Patricia Millard